ADVANCING EARTH AND SPACE SCIENCES

Geophysical Research Letters

RESEARCH LETTER

10.1029/2023GL104891

Seasonally Evolving Trends Explain the North-South Dipole Pattern Observed in Tibetan Plateau Precipitation

Jieru Ma[1], Hong-Li Ren[1], Ming Cai[2], and Jianping Huang[3]

[1]State Key Laboratory of Severe Weather, and Institute of Tibetan Plateau Meteorology, Chinese Academy of Meteorological Sciences, Beijing, China, [2]Department of Earth, Ocean, and Atmospheric Science, Florida State University, Tallahassee, FL, USA, [3]Collaborative Innovation Center for Western Ecological Safety, College of Atmospheric Sciences, Lanzhou University, Lanzhou, China

Key Points:

- Seasonally evolving patterns (SEPs) explain 60%–90% of the spatial mean amplitude of total precipitation trend over the Tibetan Plateau
- The second SEP trend with a north-south dipole pattern mainly contributes to the spatio-temporal disparity of the total precipitation trend
- The seasonally evolving north-south dipole trend is linked to the Silk Road pattern and the Indian monsoon variations

Supporting Information:

Supporting Information may be found in the online version of this article.

Correspondence to:

H.-L. Ren,
renhl@cma.gov.cn

Citation:

Ma, J., Ren, H.-L., Cai, M., & Huang, J. (2023). Seasonally evolving trends explain the north-south dipole pattern observed in Tibetan Plateau precipitation. *Geophysical Research Letters*, *50*, e2023GL104891. https://doi.org/10.1029/2023GL104891

Received 9 JUN 2023
Accepted 22 AUG 2023

Abstract

The Tibetan Plateau (TP) precipitation is experiencing the north-south dipole tendency pattern since 1979. In this study, we identify four primary seasonally evolving patterns (SEPs) that explain approximately 50% of the total variance in precipitation variability over the TP. These SEPs contribute 60%–90% of the spatial mean amplitude of precipitation trends across seasons. In particular, the second SEP that features a north-south dipole pattern dominates the annual mean trend of the precipitation over the TP. The interdecadal variability of the seasonally evolving north-south dipole pattern is linked to the interdecadal variations of summer Silk Road Pattern and Indian monsoon. These findings suggest that the climate variability expressed through SEPs could potentially serve as a significant source for the interdecadal rainfall prediction.

Plain Language Summary

The Tibetan Plateau (TP) is experiencing the north-wetting-south-drying trend due to the imbalance of the Asian water tower since 1979, influencing the water supply to billions of people and regional and global climate. However, the characteristics of the seasonally evolving variations of precipitation across seasons on multiyear timescales, as well as the associated major circulation patterns, remain unknown. Here we identify four primary seasonally evolving patterns (SEPs) and focus on investigating their corresponding long-term trends and interdecadal variations. These four modes collectively contribute by 60%–90% of the spatial mean amplitude of precipitation trends across seasons. In particular, the trend of the second SEP that features a north-south dipole explains the spatio-temporal disparity of the total precipitation trend, displaying the strongest amplitude in summer over the TP. Our findings provide insight into the climate variability manifested in SEPs as a major source for the interdecadal prediction of rainfall evolution in the Asian water tower.

1. Introduction

The water resources and hydrological cycle over the Tibetan Plateau (TP), including precipitation, glacier/snow cover, alpine lakes, and river run-off, exhibit significant and complex variations across a wide range of time scales (e.g., Immerzeel et al., 2020; Xu et al., 2008; Yao et al., 2019). Substantial efforts have been devoted to understanding the precipitation variability over the TP on interannual to interdecadal timescales and the underlying mechanisms. This variability is influenced by the tropical air-sea interactions, Asian monsoon variations, and atmospheric internal variability (e.g., Chen & You, 2017; Dong et al., 2016; Gao et al., 2013; Hu et al., 2022; Hu & Zhou, 2021; Immerzeel et al., 2010; Kang et al., 2010; Liu & Yin, 2001; Lu et al., 2015; Wang et al., 2008; Wang, Duan, et al., 2017; Yang et al., 2011). The imbalance of the Asian Water Tower, along with rapid warming in recent decades (Duan & Xiao, 2015; Ma et al., 2017; Yao et al., 2012), has caused a shift in the annual mean precipitation regimes with increased rainfall in the northern TP and decreased rainfall in the southern TP, which is referred to as the north-south dipole pattern and is associated with the anomalous westerlies and decreasing Indian monsoon (Yao et al., 2012, 2022). Additionally, there are notable decadal variations in boreal summer precipitation over the TP (Sun et al., 2020). The long-term trends and interdecadal variations of precipitation over the TP not only affect water supply for billions of people but also regulate local and surrounding climate through the release of diabatic heating (e.g., Immerzeel et al., 2010; Wu et al., 2007; Yang et al., 2014). However, current understanding and prediction capability for the seasonally evolving variations of precipitation at multiyear scales over the TP is still poor, which has imperative implications for climate prediction and local ecosystem (Kang et al., 2010; You et al., 2014).

Table 1
Monthly Precipitation Data Sets Used in This Study for the Period of 1980–2020

Number	Full name of the data set	Abbreviations	Provider	Resolution	References
1	Global Precipitation Climatology Project analysis product	GPCP	NOAA Physical Sciences Laboratory (PSL)	2.5° × 2.5°	Adler et al. (2018)
2	Climate Prediction Center merged analysis of precipitation	CMAP	NOAA PSL	2.5° × 2.5°	Xie and Arkin (1997)
3	Global Precipitation Climatology Centre precipitation data set	GPCC	NOAA PSL	0.5° × 0.5°	Schneider et al. (2017)
4	Gridded observation data set based on the interpolation of 2400 stations over China region	CN05.1	National Climate Center of China Meteorological Administration	0.25° × 0.25°	Wu and Gao (2013)
5	The fifth generation ECMWF atmospheric reanalysis of the global climate	ERA5	European Centre for Medium-Range Weather Forecasts (ECMWF)	0.25° × 0.25°	Hersbach et al. (2020)
6	The Japanese 55-year atmospheric Reanalysis project conducted by the JMA	JRA55	Japan Meteorological Agency (JMA)	1.25° × 1.25°	Harada et al. (2016)
7	Climatic Research Unit Time-Series version 4.06 of high-resolution gridded data	CRU	CRU at the University of East Anglia	0.5° × 0.5°	Harris et al. (2021)

The conventional analysis and prediction of precipitation seasonality variations at multiyear scales typically focus on the anomalies of season means with respect to the long-term mean seasonal cycle. However, this approach largely overlooks the physical premise that climate evolution across seasonal to interdecadal timescales is often modulated by the changing seasonal cycle, which can be regarded as a response to the interaction between solar radiative forcing and climate variability modes (Ma et al., 2023; Wang & An, 2005; Wu et al., 2008). Consequently, the conventional precipitation anomalies may contain a substantial component that originates from the seasonally evolving variability over the TP. Moreover, previous studies on precipitation variability over the TP have predominantly focused on summertime, paying little attention to the continuous and coherent evolution across different seasons.

Therefore, the objective of this study is to reveal the dominant seasonally evolving patterns (SEPs) of precipitation over the TP and investigate the corresponding interannual to interdecadal variations and long-term trends using an approach that considers the changing seasonal cycle. Moreover, this study investigates the associated atmospheric circulation anomalies and the possible mechanisms underlying the seasonally evolving trends of precipitation over the TP.

2. Data and Methods

2.1. Data

Multiple sources of monthly precipitation datasets are used in this study, which are listed in Table 1. We apply the multi-observation mean to the seven gridded precipitation datasets at the 2.5° resolution to reduce the uncertainty of the precipitation change in different datasets over the TP. We then apply the 5-month running mean to the multi-observation mean to filter out weather noises.

We consider monthly geopotential fields and winds at 200-hPa derived from EAR5 reanalysis (the fifth-generation reanalysis global data set from the European Centre for Medium-Range Weather Forecasts, Hersbach et al., 2020) to search for major circulation drives for the seasonally evolving trends of precipitation over the TP. The Silk Road pattern (SRP) is a typical teleconnection pattern that has pronounced interdecadal variations over the Eurasian continent in summer (Wang, Xu, et al., 2017). The SRP index is defined as the normalized principal component of the first empirical orthogonal function (EOF) mode of the summer mean 200-hPa meridional wind over the domain (20°–60°N, 30°–130°E; Kosaka et al., 2009). We also consider the Indian monsoon index (IMI) in summer defined as the difference of the 850-hPa zonal winds between the southern region of 5°–15°N, 40°–80°E and the northern region of 20°–30°N, 70°–90°E during 1980–2022 (Wang et al., 2001).

2.2. Methods

Following Ma et al. (2023), the EOF method is used to extract the yearly varying seasonal patterns of precipitation over the TP. Specifically, the monthly precipitation $P(s,t)$ after removing its long-time climatological mean, where s is spatial grid and t is time, is rearranged to the format of $P(s$, month, year). The format of $P(s$, month, year) has the advantage of reflecting both spatial and seasonal variations jointly from year to year. Applying the EOF analysis to $P(s$, month, year) with (s, month) as the space-month domain and "year" as the temporal domain yields

$$P(s, \text{month}, \text{year}) = \sum_{j=1} \text{EOF}_j(s, \text{month})\text{PC}_j(\text{year}), \text{where}\overline{(\text{PC}_j(\text{year}))^2} \equiv 1, \tag{1}$$

where the overbar denotes the 41-year (1980–2020) mean and EOF_j has the units of mm/d. In this study, the leading four EOF modes are referred to as seasonally evolving patterns (SEPs). The rainfall anomaly field associated with these SEPs is denoted as P_{SP}, which is given by

$$P_{\text{SP}}(s, \text{month}, \text{year}) = \sum_{j=1}^{4} \text{EOF}_j(s, \text{month})\text{PC}'_j(\text{year}), \tag{2}$$

where $\text{PC}'_j(\text{year}) = \text{PC}_j(\text{year}) - \overline{\text{PC}_j(\text{year})}$, and it represents the inter-annual variability of SEPs after removing the climatological seasonal cycle. Moreover, the explained variance percentage (EV_m) of the variability associated with each SEP relative to the total precipitation variability is obtained from

$$\text{EV}_m = < \text{EOF}_m(s, \text{month})^2 > \overline{\text{PC}'_m(\text{year})^2} / \sum_{j=1}^{41} \left[< \text{EOF}_j(s, \text{month})^2 > \overline{\text{PC}'_j(\text{year})^2} \right], \tag{3}$$

where $m = 1, 2, 3, 4$, and "< >" represents the average over the domain of s and month. Note that the explained variance defined in Equation 3 excludes the variability associated with the climatological seasonal cycle. As a result, the order of the explained variances by individual SEPs does not follow the order returned from the code for the EOF analysis.

To succinctly quantify the relative contributions of the monthly and spatial trend amplitudes of individual SEP to the corresponding amplitude of total precipitation trend over the TP, the pattern-amplitude projection (PAP) is used in this work, following Deng et al. (2012). The PAP coefficient is obtained from

$$\text{PAP}_\text{m} = < \Delta T > \times \frac{< \Delta T_m \Delta T >}{< (\Delta T)^2 >}, \tag{4}$$

where ΔT is the spatial pattern of total precipitation trends in each month; PAP_m and ΔT_m are the spatial PAP coefficient and partial precipitation trends of each SEP; "< >" here represents the area average over the selected TP region. The sum of all PAP_m of all EOF modes is equal to the area average of total precipitation trend. In addition, linear regression is used to investigate the atmospheric circulation patterns in summer associated with the seasonally evolving variability of major SEP.

3. Seasonally Evolving Trends of TP Precipitation

Displayed in Figure 1 are the four SEPs of the multi-observation mean precipitation anomalies derived from seven gridded observational datasets over the TP, which is similar to the patterns from station data (Figure S1 in Supporting Information S1). The SEP1 (the first row in Figure 1) is primarily characterized by a wet-dry contrast between May-September and October-April over the TP with the peak of the month-to-month spatial evolution occurring in summer and winter. The SEP1 essentially is the traditionally defined climatological seasonal cycle, representing the seasonal reversal of TP rainfall evolution. The SEP2 shows a north-south dipole mode that starts in spring and ends in autumn, representing a seasonal transition from dry to wet seasons over the northern TP starting in April and the reversal in December. The SEP2 resembles the trend patterns of the annual mean precipitation over the TP observed in recent decades (Yao et al., 2022). The SEP3 displays a dipole pattern between the southwest and northeast regions of the TP, which gradually strengthens and then weakens from spring to winter. The SEP4 exhibits a relatively uniform polarity pattern of rainfall over the TP throughout the entire year with the largest amplitude over the southeastern TP.

These four SEPs of precipitation display distinct amplitude variability across interannual to interdecadal variations and long-term trends (Figures 2a–2d), contributing to 7.5%, 16.6%, 12.5%, and 9.1% of the total variance

Geophysical Research Letters

10.1029/2023GL104891

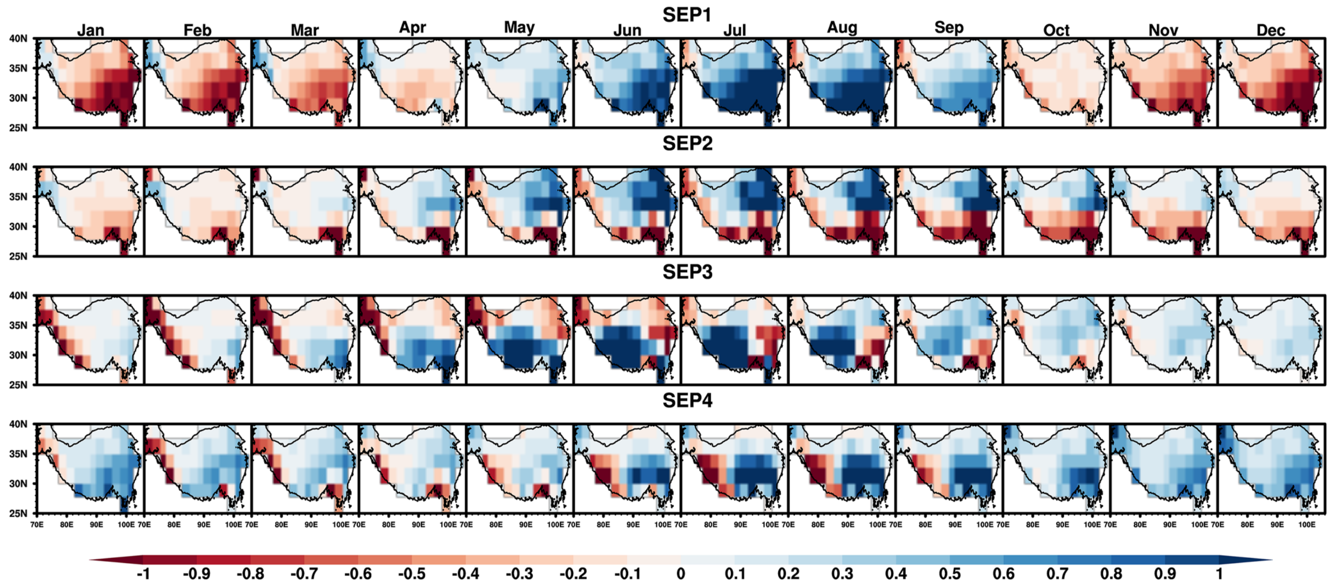

Figure 1. The seasonally evolving patterns (SEPs) of monthly mean precipitation anomalies from January to December during 1980–2020 over the Tibetan Plateau (TP). The four rows from top to bottom represent SEP1, SEP2, SEP3, and SEP4, respectively. Units of the color bar are 10 mm d^{-1} for SEP1 and mm d^{-1} for SEP2-4.

of total precipitation anomaly over the TP, respectively. The PC1 and PC4 exhibit strong interannual variability whereas the PC2 and PC3 show interdecadal variability. Meanwhile, the amplitude variations of all four PCs exhibit varying degrees of long-term trends. Collectively, the variations of these four SEPs (i.e., P_{SP}) account for approximately 50% of the total variance in precipitation variability (Figure 2e), with the corresponding center of the spatial change maxima located in the northern and southern regions of the TP (Figure 2f). Figures S2–S6 in Supporting Information S1 also show the performance of SEPs and PCs from seven individual gridded datasets, and SEPs and PCs of the multi-observation mean have better spatial and temporal correspondences with that from the station-based data (Figure S1 in Supporting Information S1). Meanwhile, the main SEPs and amplitude variability remain generally consistent when using station-based data from 1961 to 2020, although there are fewer observations before 1980.

Since 1979, the annual mean precipitation of Asian water tower has undergone a north-south dipole trend pattern (Yao et al., 2012, 2022). However, the extent to which the aforementioned SEP trend pattern contribute to the continuous spatio-temporal evolution of precipitation trends over the TP remains unclear. It is seen in Figure 2b that upward trend of the PC2 is the dominant signal of its interdecadal variability, suggesting the potential significance in shaping the north-south dipole pattern observed in the overall precipitation trends over the TP. Shown in Figure 3 are the seasonally evolving trend patterns of precipitation over the TP derived from the four SEPs and the original total precipitation field in 1980–2020. The seasonal pattern associated with the SEP1 exhibits a weak drier winter and wetter summer in the southwestern TP, whereas the SEP2 trend pattern closely aligns with the spatial dipole pattern of the total precipitation trend. The SEP3 trend pattern is characterized with the wet in the southwestern TP but the dry in the northeastern TP from spring to autumn, and a dry condition in the Himalayas during winter. The SEP4 trend pattern exhibits a more rainfall pattern in the southeastern TP and a drier condition in the Himalayas, which is most pronounced in summer and weakens in other seasons.

To assess the relative contributions of seasonally evolving dominant patterns to the spatial mean amplitude of precipitation trends over the TP, we calculate the monthly pattern-amplitude projection (PAP_m) of partial trends using the total precipitation and four SEPs, as illustrated in Figure 4. The spatial mean amplitude of the total precipitation trend increases from a minimum value of 8 mm/decade in winter to a maximum value of 25 mm/decade in summer (the red line in Figure 4a). It is seen that the trends of the four SEPs account for 60%–90% of the spatial mean amplitude of the total precipitation trend from spring to autumn (Figure 4b or the blue line in Figure 4a). In particularly, the spatial mean amplitude of the SEP2 trend explains more than half of the counterparts of the total precipitation trend during summer. Despite that these four SEPs explain only about 50% of the total variance of the precipitation variability (Figure 2e), they collectively account for nearly 80% of the annual

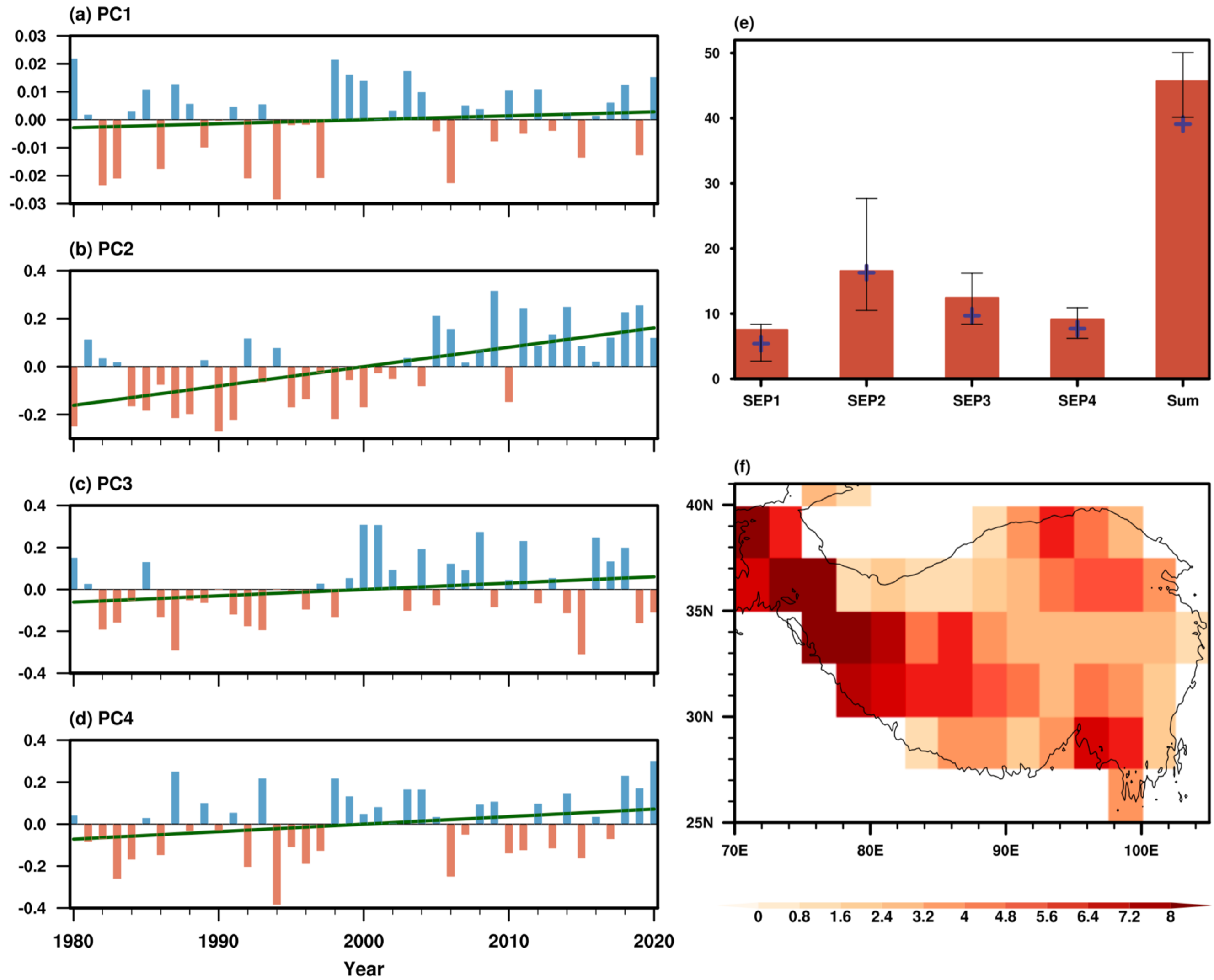

Figure 2. (a)–(d) The variability of normalized principal components (PCs) corresponding to the four seasonally evolving patterns (SEPs) of precipitation over the Tibetan Plateau (TP) from 1980 to 2020; (e) The percentage variance (unit: %) of precipitation variability explained by four SEPs and their combined contribution derived from the mean of seven datasets with the thin black line segments for their ranges derived from individual datasets; (f) is the same as (e), but for the spatial distribution of percentage variance explained by the seasonal variation reconstructed from the four SEPs and PCs. The symbol "+" in panel (e) represents the counterpart results derived from station data.

and spatial mean amplitude of the total precipitation trend over the TP with 70% coming from the SEP2 trend (Figure 4c).

4. Possible Factors for the Seasonally Evolving Trends

We next examine the circulation anomalies in summer seasons that are linked to the interdecadal variability and trends of precipitation over the TP. Shown in Figures 5a and 5b, respectively, are the trends of the summer mean precipitation anomalies over the TP and 200 hPa eddy geopotential height anomalies. As expected from the results shown in Figure 4, the trends of the summer mean precipitation anomalies can be approximately represented by the product of the trend of PC2 and the SEP2 pattern in summer (Figure 5c). The regressed pattern of 200 hPa eddy geopotential height anomalies against PC2 (Figure 5d) resembles the spatial pattern shown in Figure 5b, strongly suggesting the association of the trend of the SEP2 with the trends of 200 hPa eddy geopotential height anomalies. The positive trends of the anticyclone over the northeastern TP and anomalous cyclone over the western TP contribute to the formation of a north-south dipole pattern in summer rainfall, leading to increased (decreased) variations of rainfall over the northern (southern) TP.

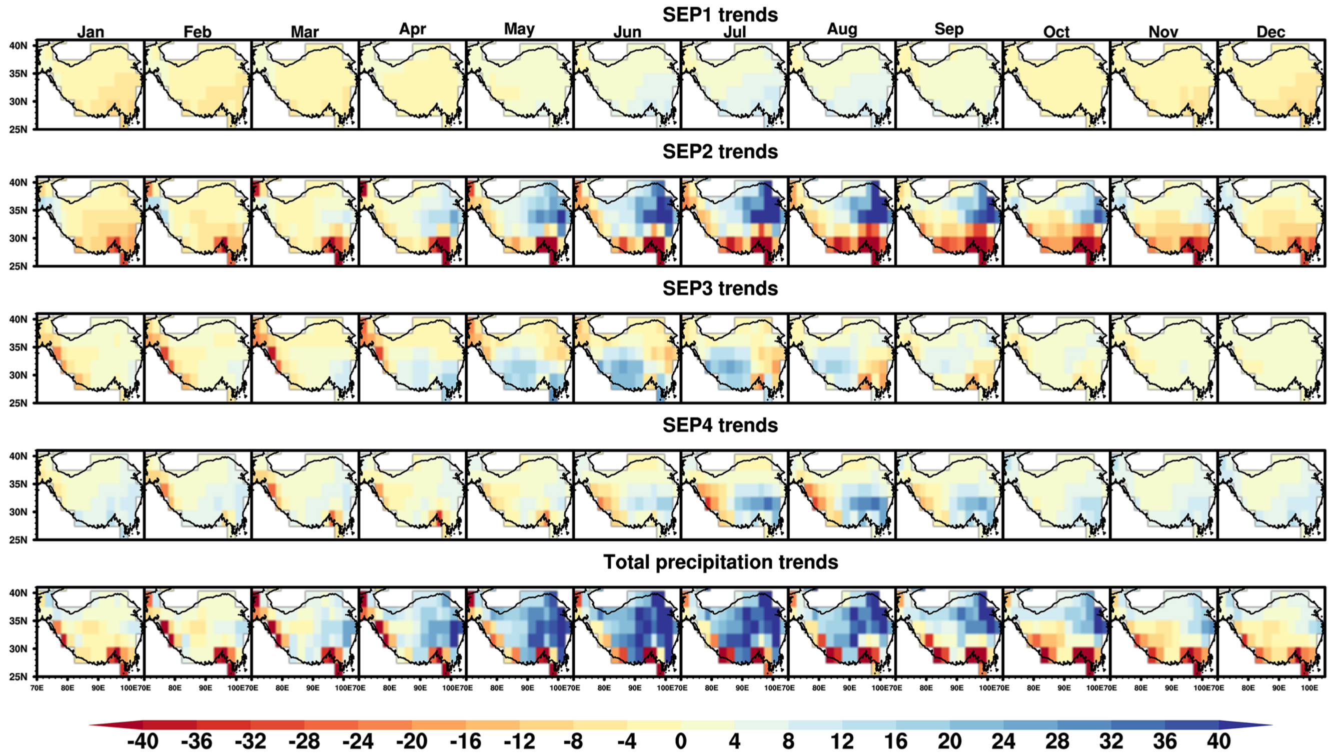

Figure 3. Patterns from the top to bottom rows represent the seasonal evolution of monthly trends from January to December using the four seasonally evolving patterns (SEPs) and total variability of precipitation in the Tibetan Plateau (TP) during 1980–2020, respectively. The values on the color bar are given in units of mm decade^{-1}.

Previous studies have shown that the Silk Road pattern (SRP) (e.g., Hu & Zhou, 2021; Sun et al., 2020; Wu et al., 2016; Zhou et al., 2019) and Indian monsoon index (IMI) variations (e.g., Dong et al., 2016; Kong & Chiang, 2020; Mölg et al., 2014; Yao et al., 2012) during summer have a significantly impact on the TP climate by influencing the westerly jet stream and water vapor transport on the interdecadal time scales. It is seen from Figures 5e and 5g. The regressed patterns of the summer mean rainfall anomalies against the SRP and IMI indices exhibit a similar spatial pattern as the summer mean pattern of total precipitation trend as well as the summer pattern of SEP2. The regressed pattern of 200 hPa eddy geopotential height anomalies against these two indices (Figures 5f and 5h) also show a similar spatial pattern as their counterpart obtained from the regression against the PC2. There are some noticeable differences in the upper-level teleconnection pattern associated with SRP from that associated with IMI. The former (Figure 5f) exhibits an eastward-propagating wave train across the TP whereas the latter show a wave train located further south. According to Hu and Zhou (2021) and Sun et al. (2020), the interdecadal SRP wave trains near the TP may originate from the sea surface temperature anomalies over the North Atlantic. The anomalous anticyclone over northeast of the TP results in a northward shift and/or weakening of the jet stream in that region. This leads to a reduction in the water vapor transport out of the TP through its eastern boundary. The anomalous cyclone to the northwest of the TP, on the other hand, causes a more meandered jet stream over the western TP, resulting in more meridional transport of water vapor from the Arabian Sea into the inner TP. Additionally, the weakening of the Indian monsoon since the 1980s, possible associated with SST anomalies in the Indian and central Pacific oceans (Yue et al., 2020), results in a reduction of moisture transport from Indian oceans across the Indian subcontinent. This reduction contributes to the decreasing rainfall trend in the southwestern TP (Dong et al., 2016; Yao et al., 2022).

The anomalous anticyclones (cyclones) in the mid-latitude associated with SRP provide a favorable environment condition for the increasing of rainfall in the inner and northern TP (Figures 5e and 5f), while the low-latitude wave patterns related to IMI are favorable for dry season in the southwestern TP and wet season in the northeastern TP (Figures 5g and 5h). Overall, the combined effect of mid-latitude and low-latitude circulation patterns associated with SRP and IMI plays an important role in generating anticyclonic anomalies on the west and cyclonic anomalies on the east of the TP, regulating the westerly jet stream and water vapor transport passing

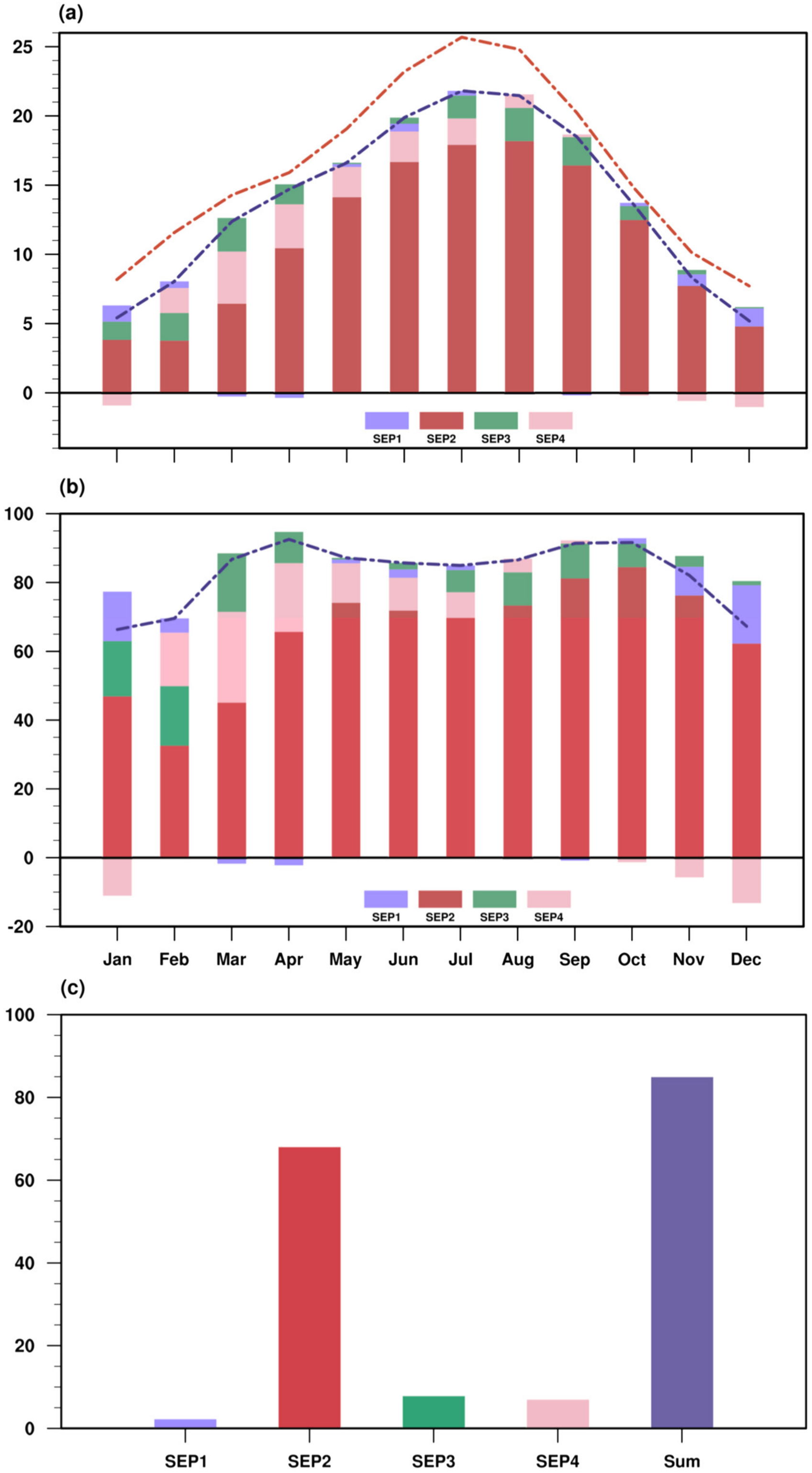

Figure 4. (a) The monthly pattern-amplitude projection (PAPs) coefficients (ordinate, unit: mm decade^{-1}) of the spatial mean amplitudes of trends as a function of months (abscissa), using each seasonally evolving patterns (SEPs, color bars), their sum (blue line) and the total precipitation (red line) over the Tibetan Plateau (TP). (b) Similar to (a), but for the relative PAP contributions (unit: %) of the spatial mean amplitude of each SEP trend relative to that of the total precipitation trend. (c) Similar to (b), but for the annual mean of the PAP. The color bars, stacked vertically, are arranged from bottom to top based on the decreasing absolute value of the PAPs portion for individual SEP.

10.1029/2023GL104891

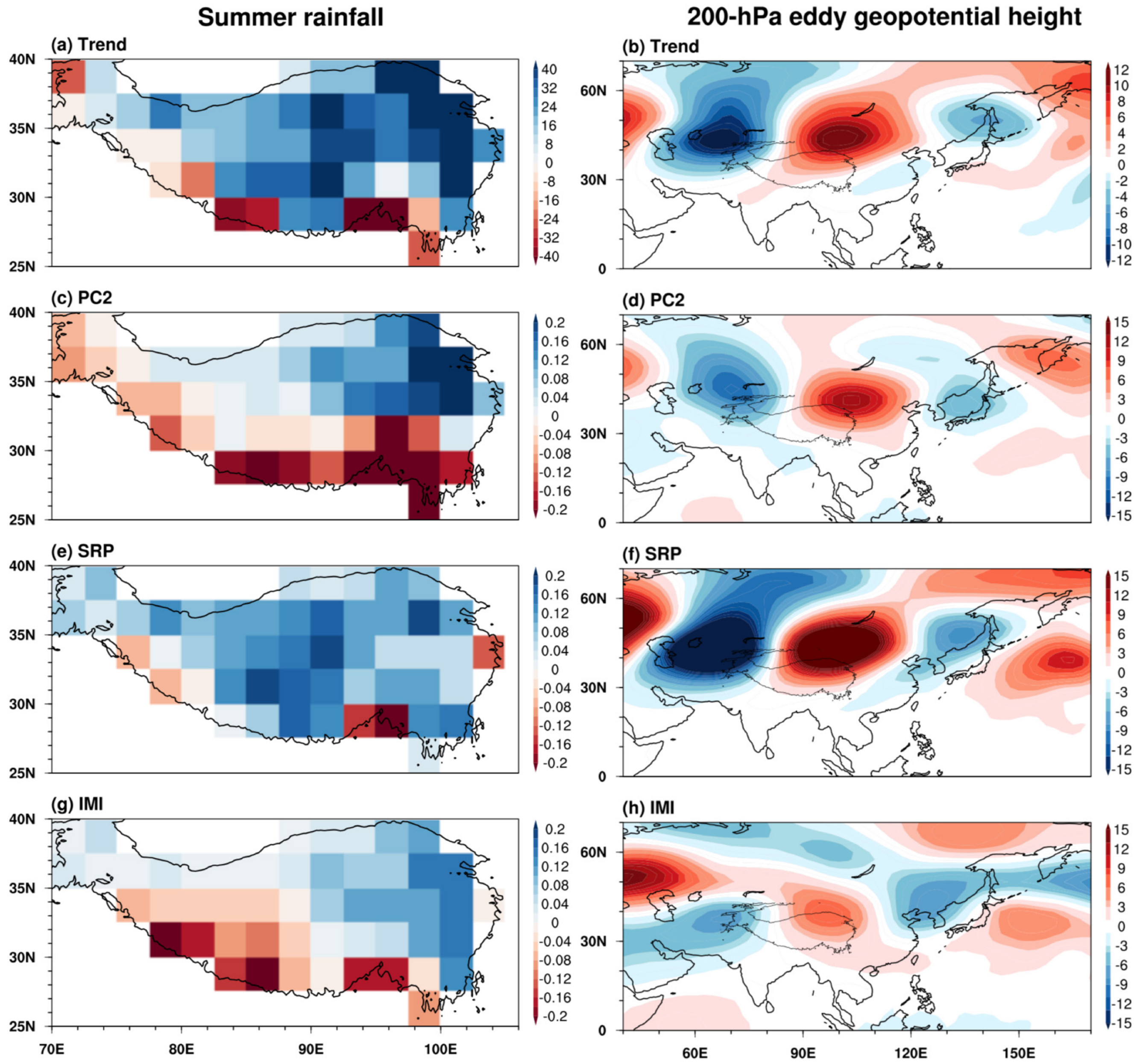

Figure 5. The observed trends of (a) TP rainfall (unit: mm decade^{-1}) and (b) 200-hPa eddy geopotential height (with zonal mean removed, unit: m decade^{-1}) in summer during 1980–2020. The regressed patterns of summer rainfall (left panels, unit: mm d^{-1}) and 200-hPa eddy geopotential height anomalies (right panels, unit: m) against the variability of (c, d) the second principal component (PC2), (e, f) the Silk Road pattern (SRP) index, and (g, h) the negative Indian monsoon index (IMI).

through the TP (e.g., Dong et al., 2016; Hu & Zhou, 2021; Yao et al., 2022). The trends of these circulation anomalies lead to the north-south dipole trend of seasonal rainfall patterns over the TP. It is of importance to point out that the north-south dipole trend is pronounced mainly in summer. In other seasons, the north-south dipole pattern has a weak relationship with the circulation patterns associated with SRP and IMI (Figures S7 and S8 in Supporting Information S1).

5. Summary

We here identify four yearly varying seasonal evolving patterns (SEPs) of the precipitation field over the TP in the period of 1980–2020 by applying the EOF analysis in the space-month domain for seasonal evolving patterns and year as the temporal domain for their yearly time series. These patterns are characterized by the distinct seasonal reversal, transition in spatio-temporal domain, and they collectively explain approximately 50% of the total variance of the precipitation field over the TP and 60%–90% of the spatial mean amplitude of the total precipitation trend in the seasons of spring, summer, autumn and winter. In particularly, the second SEP that features a north-south dipole is the primary contributor to the distinct north-south trend pattern observed in the annual mean precipitation field over the TP. The second SEP is associated with an anticyclone over the northeastern TP and an anomalous cyclone over the western TP, which are in turn are linked to the interdecadal variability of the Silk Road pattern (SRP) and Indian monsoon (IMI) indices.

The findings of this study demonstrate that the interdecadal variations and long-term trends of TP rainfall are modulated by the year-to-year seasonal pattern variability. Moreover, the association of the rainfall SEPs over the TP with SRP and IMI variability could potentially serve as a significant source for predicting interdecadal climate of seasonal evolution of rainfall over the TP with a long lead-time as demonstrated in Ma et al. (2023) for skillful seasonal forecasts of precipitation over eastern China.

Conflict of Interest

The authors declare no conflicts of interest relevant to this study.

Data Availability Statement

The precipitation datasets shown in Table 1 are available at https://psl.noaa.gov/data/gridded/data.gpcp.html for GPCP, https://psl.noaa.gov/data/gridded/data.cmap.html for CMAP, https://psl.noaa.gov/data/gridded/data.gpcc.html for GPCC, https://cds.climate.copernicus.eu/cdsapp#!/dataset/reanalysis-era5-single-levels-monthly-means?tab=form for ERA5, https://rda.ucar.edu/datasets/ds628.1/dataaccess/ for JRA55, and https://crudata.uea.ac.uk/cru/data/hrg/cru_ts_4.06/cruts.2205201912.v4.06/pre/ for CRU. The CN05.1 precipitation data was obtained by the authors through an agreement with the China Meteorological Administration for the present study, and is not publicly available. The ERA5 geopotential and wind fields are available at https://cds.climate.copernicus.eu/cdsapp#!/dataset/reanalysis-era5-pressure-levels-monthly-means?tab=form. Indian monsoon index is available at http://apdrc.soest.hawaii.edu/projects/monsoon/seasonal-monidx.html.

Acknowledgments

This work was supported by the National Natural Science Foundation of China (Grant U2242206) and Special Project for Innovation and Development of CMA (Grant CXFZ2023J050).

References

Adler, R., Sapiano, M., Huffman, G., Wang, J., Gu, G., Bolvin, D., et al. (2018). The global precipitation climatology project (GPCP) monthly analysis (new version 23) and a review of 2017 global precipitation. *Atmosphere*, *9*(4), 138. https://doi.org/10.3390/atmos9040138

Chen, X., & You, Q. (2017). Effect of Indian Ocean SST on Tibetan Plateau precipitation in the early rainy season. *Journal of Climate*, *30*(22), 8973–8985. https://doi.org/10.1175/JCLI-D-16-0814.1

Deng, Y., Park, T., & Cai, M. (2012). Process-based decomposition of the global surface temperature response to El Niño in boreal winter. *Journal of the Atmospheric Sciences*, *69*(5), 1706–1712. https://doi.org/10.1175/JAS-D-12-023.1

Dong, W., Lin, Y., Jonathon, S., Ming, Y., Xie, Y., Wang, B., et al. (2016). Summer rainfall over the southwestern Tibetan Plateau controlled by deep convection over the Indian subcontinent. *Nature Communications*, *7*(1), 10925. https://doi.org/10.1038/ncomms10925

Duan, A., & Xiao, Z. (2015). Does the climate warming hiatus exist over the Tibetan Plateau? *Scientific Reports*, *5*(1), 13711. https://doi.org/10.1038/srep13711

Gao, Y., Wang, H., & Li, S. (2013). Influences of the Atlantic Ocean on the summer precipitation of the southeastern Tibetan Plateau. *Journal of Geophysical Research: Atmospheres*, *118*(9), 3534–3544. https://doi.org/10.1002/jgrd.50290

Harada, Y., Kamahori, H., Kobayashi, C., Endo, H., Kobayashi, S., Ota, Y., et al. (2016). The JRA-55 Reanalysis: Representation of atmospheric circulation and climate variability. *Journal of the Meteorological Society of Japan*, *94*(3), 269–302. https://doi.org/10.2151/jmsj.2016-015

Harris, I. C., Jones, P. D., & Osborn, T. (2021). *CRU TS4.05: Climatic research unit (CRU) time-series (TS) version 4.05 of high-resolution gridded data of month-by-month variation in climate (January 1901–December 2020)*. NERC EDS Centre for Environmental Data Analysis. Retrieved from https://catalogue.ceda.ac.uk/uuid/c26a65020a5e4b80b

Hersbach, H., Bell, B., Berrisford, P., Hirahara, S., Horányi, A., Muñoz-Sabater, J., et al. (2020). The ERA5 global reanalysis. *Quarterly Journal of the Royal Meteorological Society*, *146*(730), 1999–2049. https://doi.org/10.1002/qj.3803

Hu, S., & Zhou, T. (2021). Skillful prediction of summer rainfall in the Tibetan Plateau on multiyear time scales. *Science Advances*, *7*(24), eabf9395. https://doi.org/10.1126/sciadv.abf9395

Hu, S., Wu, B., Zhou, T., & Yu, Y. (2022). Dominant anomalous circulation patterns of Tibetan Plateau summer climate generated by ENSO-forced and ENSO-independent teleconnections. *Journal of Climate*, *35*(5), 1679–1694. https://doi.org/10.1175/JCLI-D-21-0207.1

Immerzeel, W., Lu, A., Andrade, M., Bahl, A., Biemans, H., Bolch, T., et al. (2020). Importance and vulnerability of the world's water towers. *Nature*, *577*(7790), 364–369. https://doi.org/10.1038/s41586-019-1822-y

Immerzeel, W., Van Beek, L., & Bierkens, M. (2010). Climate change will affect the Asian water towers. *Science*, *328*(5984), 1382–1385. https://doi.org/10.1126/science.1183188

Kang, S., Xu, Y., You, Q., Flügel, W., Pepin, N., & Yao, T. (2010). Review of climate and cryospheric change in the Tibetan Plateau. *Environmental Research Letters*, *5*(1), 015101. https://doi.org/10.1088/1748-9326/5/1/015101

Kong, W., & Chiang, J. C. H. (2020). Southward shift of westerlies intensifies the East Asian early summer rainband following El Niño. *Geophysical Research Letters*, *47*(17), e2020GL088631. https://doi.org/10.1029/2020GL088631

Kosaka, Y., Nakamura, H., Watanabe, M., & Kimoto, M. (2009). Analysis on the dynamics of a wave-like teleconnection pattern along the summertime Asian jet based on a reanalysis dataset and climate model simulations. *Journal of the Meteorological Society of Japan*, *87*(3), 561–580. https://doi.org/10.2151/jmsj.87.561

Liu, X., & Yin, Z. (2001). Spatial and temporal variation of summer precipitation over the eastern Tibetan Plateau and the North Atlantic Oscillation. *Journal of Climate*, *14*(13), 2896–2909. https://doi.org/10.1175/1520-0442(2001)014<2896:SATVOS>2.0.CO;2

Lu, N., Trenberth, K. E., Qin, J., Yang, K., & Yao, L. (2015). Detecting long-term trends in precipitable water over the Tibetan Plateau by synthesis of station and MODIS observations. *Journal of Climate*, *28*(4), 1707–1722. https://doi.org/10.1175/JCLI-D-14-00303.1

Ma, J., Guan, X., Guo, R., Gan, Z., & Xie, Y. (2017). Mechanism of non-appearance of hiatus in Tibetan Plateau. *Scientific Reports*, *7*(1), 4421. https://doi.org/10.1038/s41598-017-04615-7

Ma, J. R., Sun, J., Wu, Z. H., Huang, J. P., Xu, X. F., Deng, Y., & Cai, M. (2023). Pushing the boundary of seasonal prediction with the lever of varying annual cycles. *Science Bulletin*, *68*(1), 105–116. https://doi.org/10.1016/j.scib.2022.12.026

Mölg, T., Maussion, F., & Scherer, D. (2014). Mid-latitude westerlies as a driver of glacier variability in monsoonal High Asia. *Nature Climate Change*, *4*(1), 68–73. https://doi.org/10.1038/nclimate2055

Schneider, U., Finger, P., Meyer-Christoffer, A., Rustemeier, E., Ziese, M., & Becker, A. (2017). Evaluating the hydrological cycle over land using the newly-corrected precipitation climatology from the Global Precipitation Climatology Centre (GPCC). *Atmosphere*, *8*(3), 52. https://doi.org/10.3390/atmos8030052

Sun, J., Yang, K., Guo, W., Wang, Y., He, J., & Lu, H. (2020). Why has the inner Tibetan Plateau become wetter since the mid-1990s? *Journal of Climate*, *33*(19), 8507–8522. https://doi.org/10.1175/JCLI-D-19-0471.1

Wang, B., & An, S. (2005). A method for detecting season-dependent modes of climate variability: S-EOF analysis. *Geophysical Research Letters*, *32*(15), L15710. https://doi.org/10.1029/2005GL022709

Wang, B., Bao, Q., Hoskins, B., Wu, G., & Liu, Y. (2008). Tibetan Plateau warming and precipitation changes in East Asia. *Geophysical Research Letters*, *35*(14), L14702. https://doi.org/10.1029/2008GL034330

Wang, B., Wu, R., & Lau, K. (2001). Interannual variability of Asian summer monsoon: Contrast between the Indian and western North Pacific-East Asian monsoons. *Journal of Climate*, *14*(20), 4073–4090. https://doi.org/10.1175/1520-0442(2001)014<4073:IVOTAS>2.0.CO;2

Wang, L., Xu, P., Chen, W., & Liu, Y. (2017). Interdecadal variations of the Silk Road pattern. *Journal of Climate*, *30*(24), 9915–9932. https://doi.org/10.1175/JCLI-D-17-0340.1

Wang, Z., Duan, A., Yang, S., & Ullah, K. (2017). Atmospheric moisture budget and its regulation on the variability of summer precipitation over the Tibetan Plateau. *Journal of Geophysical Research: Atmospheres*, *122*(2), 614–630. https://doi.org/10.1002/2016JD025515

Wu, B., Lin, J., & Zhou, T. (2016). Interdecadal circumglobal teleconnection pattern during boreal summer. *Atmospheric Science Letters*, *17*(8), 446–452. https://doi.org/10.1002/asl.677

Wu, G., Liu, Y., Zhang, Q., Duan, A., Wang, T., Wan, T., et al. (2007). The influence of mechanical and thermal forcing by the Tibetan Plateau on Asian climate. *Journal of Hydrometeorology*, *8*(4), 770–789. https://doi.org/10.1175/JHM609.1

Wu, J., & Gao, X. (2013). A gridded daily observation dataset over China region and comparison with the other datasets. *Chinese Journal of Geophysics*, *56*(4), 1102–1111. (in Chinese). https://doi.org/10.6038/cjg20130406

Wu, Z., Schneider, E., Kirtman, B., Kirtman, B., Sarachik, E., Huang, N., & Tucker, C. (2008). The modulated annual cycle: An alternative reference frame for climate anomalies. *Climate Dynamics*, *31*(7–8), 823–841. https://doi.org/10.1007/s00382-008-0437-z

Xie, P., & Arkin, P. (1997). Global precipitation: A 17-year monthly analysis based on gauge observations, satellite estimates, and numerical model outputs. *Bulletin of the American Meteorological Society*, *78*(11), 2539–2558. https://doi.org/10.1175/1520-0477(1997)078<2539:GPAYMA>2.0.CO;2

Xu, X., Lu, C., Shi, X., & Gao, S. (2008). World water tower: An atmospheric perspective. *Geophysical Research Letters*, *35*(20), L20815. https://doi.org/10.1029/2008GL035867

Yang, K., Wu, H., Qin, J., Lin, C., Tang, W., & Chen, Y. (2014). Recent climate changes over the Tibetan Plateau and their impacts on energy and water cycle: A review. *Global and Planetary Change*, *112*, 79–91. https://doi.org/10.1016/j.gloplacha.2013.12.001

Yang, K., Ye, B., Zhou, D., Wu, B., Foken, T., Qin, J., & Zhou, Z. (2011). Response of hydrological cycle to recent climate changes in the Tibetan Plateau. *Climatic Change*, *109*(3–4), 517–534. https://doi.org/10.1007/s10584-011-0099-4

Yao, T., Bolch, T., Chen, D., Gao, J., Immerzeel, W., Piao, S., et al. (2022). The imbalance of the Asian water tower. *Nature Reviews Earth & Environment*, *3*(10), 618–632. https://doi.org/10.1038/s43017-022-00299-4

Yao, T., Thompson, L., Yang, W., Yu, W., Gao, Y., Guo, X., et al. (2012). Different glacier status with atmospheric circulations in Tibetan Plateau and surroundings. *Nature Climate Change*, *2*(9), 663–667. https://doi.org/10.1038/nclimate1580

Yao, T., Xue, Y., Chen, D., Chen, F., Thompson, L., Cui, P., et al. (2019). Recent Third Pole's rapid warming accompanies cryospheric melt and water cycle intensification and interactions between monsoon and environment: Multidisciplinary approach with observations, modeling, and analysis. *Bulletin of the American Meteorological Society*, *100*(3), 423–444. https://doi.org/10.1175/BAMS-D-17-0057.1

You, Q., Min, J., Zhang, W., Pepin, N., & Kang, S. (2014). Comparison of multiple datasets with gridded precipitation observations over the Tibetan Plateau. *Climate Dynamics*, *45*(3–4), 791–806. https://doi.org/10.1007/s00382-014-2310-6

Yue, S., Wang, B., Yang, K., Xie, Z., Lu, H., & He, J. (2020). Mechanisms of the decadal variability of monsoon rainfall in the southern Tibetan Plateau. *Environmental Research Letters*, *16*(1), 014011. https://doi.org/10.1088/1748-9326/abcb36

Zhou, C., Zhao, P., & Chen, J. (2019). The interdecadal change of summer water vapor over the Tibetan Plateau and associated mechanisms. *Journal of Climate*, *32*(13), 4103–4119. https://doi.org/10.1175/JCLI-D-18-0364.1